9th U. S. National Combustion Meeting
Organized by the Central States Section of the Combustion Institute
May17-20, 2015
Cincinnati, Ohio

Combustion Characteristics in a Non-Premixed Cool-Flame Regime of n-Heptane in Microgravity

Fumiaki Takahashi[1,], Viswanath R. Katta[2], Michael C. Hicks[3]*

[1]Case Western Reserve University, 10900 Euclid Avenue, Cleveland, OH, USA
[2]Innovative Scientific Solutions, Inc., 7610 McEwen Road, Dayton, OH, USA
[3]NASA Glenn Research Center, 21000 Brookpark Rd, Cleveland, OH, USA
[*]Corresponding Author Email: fxt13@case.edu

Abstract: A series of distinct phenomena have recently been observed in single-fuel-droplet combustion tests performed on the International Space Station (ISS). This study attempts to simulate the observed flame behavior numerically using a gaseous n-heptane fuel source in zero gravity and a time-dependent axisymmetric (2D) code, which includes a detailed reaction mechanism (127 species and 1130 reactions), diffusive transport, and a radiation model (for CH_4, CO, CO_2, H_2O, and soot). The calculated combustion characteristics depend strongly on the air velocity around the fuel source. In a near-quiescent air environment (≤ 2 mm/s), with a sufficiently large fuel injection velocity (1 cm/s), a growing spherical diffusion flame extinguishes at ≈1200 K due to radiative heat losses. This is typically followed by a transition to the low-temperature (cool-flame) regime with a reaction zone (at ≈700 K) in close proximity to the fuel source. The 'cool flame' regime is formed due to the negative temperature coefficient in the low-temperature chemistry. After a relatively long period (≈18 s) of the cool flame regime, a flash re-ignition occurs, associated with flame-edge propagation and subsequent extinction of the re-ignited flame. In a low-speed (≈3 mm/s) airstream (which simulates the slight droplet movement), the diffusion flame is enhanced upstream and experiences a local extinction downstream at ≈1200 K, followed by steady flame pulsations (≈0.4 Hz). At higher air velocities (4−10 mm/s), the locally extinguished flame becomes steady state. The present axisymmetric computational approach helps in revealing the non-premixed 'cool flame' structure and 2D flame-flow interactions observed in recent microgravity droplet combustion experiments.

Keywords: *diffusion flame, droplet combustion, negative temperature coefficient, pulsating flame*

1. Introduction

Since 1950's, microgravity droplet combustion experiments and related spherically symmetric model descriptions have uncovered new and important phenomena that are generally obscured in normal gravity [1, 2]. In recent droplet combustion tests performed in the Flame Extinguishment Experiment (FLEX) on the International Space Station (ISS), a series of distinct phenomena have been observed. As it has long been known, a spherical diffusion flame of a relatively large n-alkane droplet in microgravity grows and extinction occurs due to radiative heat losses. It has recently been discovered that the droplet can continue to burn quasi-steadily [3]. The second-stage combustion of the droplet is due to the negative temperature coefficient in the low-temperature chemistry. This low-temperature burning is generally referred to as a 'cool flame' regime. After a relatively long period of the cool flame regime, a flash re-ignition, followed by flame-edge propagation and subsequent extinction of the re-ignited flame can occur when the

atmospheric pressure is slightly elevated. Furthermore, flame pulsations have also been observed during conditions when the droplet is slowly moving so that there is a relative velocity between the gas phase and the droplet.

Spherically symmetric (one-dimensional) simulations with a detailed chemistry were performed [4–6] to simulate successfully the two-stage combustion phenomena observed in the droplet combustion experiments. The slight droplet movement induces relative convection and, in turn, two-dimensional (2D) flame-flow interactions: local extinction, pulsation, flame propagation after re-ignition, and local soot formation. Since the flame-flow interactions are controlled primarily by the physical and chemical processes in the gas phase, the series of events can be studied by using a gaseous fuel flame. In addition, unlike a depleting isolated fuel droplet, the gaseous fuel can be supplied indefinitely to explore the steadiness or long-term variations in the phenomenon under study. In this study, axisymmetric 2D computation is performed with a detailed n-heptane reaction mechanism to simulate the two-stage combustion phenomena and the flame-flow interactions using a gaseous fuel source in zero gravity. The objectives of this study are to gain a better understanding of a series of the events: (1) the two-stage combustion—flame expansion, radiative extinction, cool-flame formation, re-ignition, flame propagation; and (2) convection effects—local extinction, flame pulsation, and local soot formation.

2. Computational Methods

A time-dependent, axisymmetric numerical code (UNICORN) [7, 8] is used for the simulation of diffusion flames stabilized on an axisymmetric burner in zero gravity. The code solves the axial and radial (z and r) full Navier-Stokes momentum equations, continuity equation, and enthalpy- and species-conservation equations on a staggered-grid system. A clustered mesh system is employed to trace the gradients in flow variables near the flame surface. The thermo-physical properties such as enthalpy, viscosity, thermal conductivity, and binary molecular diffusion of all of the species are calculated from the polynomial curve fits developed for the temperature range 300 K to 5000 K. Mixture viscosity and thermal conductivity are then estimated using the Wilke and Kee expressions, respectively. Molecular diffusion is assumed to be of the binary-diffusion type, and the diffusion velocity of a species is calculated using Fick's law and the effective-diffusion coefficient of that species in the mixture.

A comprehensive reaction mechanism (the Curran mechanism [9] reduced by Farouk & Dryer [5]; 127 species and 1130 reactions) is integrated into the UNICORN code for the simulation of n-heptane flames in zero gravity. The PAH mechanism was added for the prediction of soot. While the UNICORN model with various chemistries was extensively validated in the past through simulating steady and unsteady counterflow and coflow jet diffusion flames, the integration of heptane and PAH chemistries was validated [10] by simulating counterflow partially premixed flames of Berta et al. [11]. Predictions for temperature and various species including benzene matched well with the measurements [11].

A simple radiation model based on the optically thin-media assumption is incorporated into the energy equation [12]. Only radiation from CH_4, CO, CO_2, H_2O and soot is considered in the present study. The two-equation approach of Lindstedt [13, 14] that describes soot distribution using transport equations for soot mass fraction and number density is used. The source terms in

the soot equations were obtained based on the assumption that nucleation and growth are first-order functions of acetylene concentrations.

The finite-difference forms of the momentum equations are obtained using an implicit QUICKEST scheme [7], and those of the species and energy equations are obtained using a hybrid scheme of upwind and central differencing. At every time-step, the pressure field is accurately calculated by solving all the pressure Poisson equations simultaneously and using the LU (Lower and Upper diagonal) matrix-decomposition technique.

Unsteady axisymmetric calculations for porous burner flames are made on a physical domain of 200 mm by 100 mm using a 301 × 151 non-uniform grid system that yields 0.1 mm by 0.1 mm minimum grid spacing in the z and r directions, respectively, in the flame zone. The computational domain is bounded by the axis of symmetry and a chimney wall boundary in the radial direction and by the inflow and outflow boundaries in the axial direction. The outflow boundary in z direction is located sufficiently far from the burner (~50 burner radii) such that propagation of boundary-induced disturbances into the region of interest is minimal. Flat velocity profiles are imposed at the air inflow boundaries, while an extrapolation procedure with weighted zero- and first-order terms is used to estimate the flow variables at the outflow boundary.

Axisymmetric fuel sources (a porous cylinder and superimposed two or three cylinders), suitable for the UNICON code's rectilinear grid system, are used. In this paper, unless otherwise noted, only results obtained for the three-cylinder burner (Fig. 1) are presented. The fuel source consists of three superimposed porous cylinders (4 mm dia. × 0.67 mm ht., 2.5 mm dia. × 2 mm ht., and 1 mm dia. × 4 mm ht.). The surface areas in the axial and radial directions are equal ($2\pi r^2$, r = 2 mm), and the total surface area ($4\pi r^2$) is equal to that of a sphere with the same radius. First, gaseous n-heptane under the saturation vapor pressure at a room temperature (293 K) diffuses from the burner surface without convection for a fixed pre-ignition period (0.2 to 600 s). The effect of the pre-ignition period is weak, and only results obtained for 1 s is reported here. The stoichiometric mixture is ignited at locations on the centerline upstream and downstream of the burner. At ignition, the burner wall and fuel temperatures are set at the boiling point of n-heptane (372 K). The fuel velocity is set at 1 cm/s, which corresponds to the combustion of a 4.4 mm-diameter droplet at a 0.5 mm^2/s burning-rate constant. The airstream velocity is varied between 0 and 1 cm/s, and the air temperature is set at 300 K.

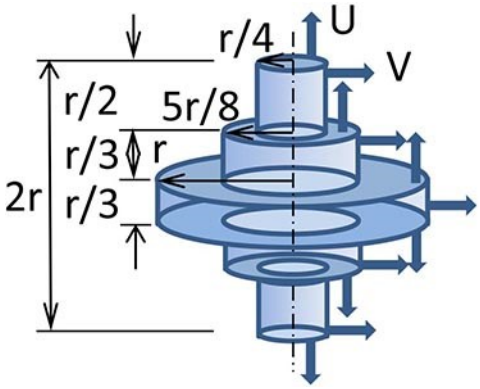

Figure 1: Schematic illustration of the axisymmetric porous burner

3. Results and Discussion

Two-Stage Combustion

In the present computation, the stoichiometric fuel-air mixture is ignited on the centerline upstream and downstream of the burner after the pre-diffusion period of 1 s. The flame edges propagate around the fuel source and merge together to form a small (≈10 mm dia.) spherical diffusion flame. The diffusion flame expands outwardly and extinguishes eventually. Figure 2 shows the calculated structure of zero-gravity n-heptane flames in quiescent air. The variables include the velocity vectors ($\boldsymbol{v}$) and isotherms (T) on the right, and the heat-release rate (HRR, $\dot{q}$) and the oxygen mole fraction (X_{O2}) on the left. Figure 2a shows a flame just before extinction by radiative heat losses at the elapse time from ignition t = 6 s. The flame is spherical with a diameter of ≈37 mm, without any influence by the non-spherical fuel source. All velocity vectors show radial directions (i.e., spherical symmetry). The maximum temperature is 1235 K. The peak HRR exhibits some decrease (1.6 ± 0.1 W/cm^3) along the flame downstream, presumably due to initial enhanced soot formation on the downstream side. The oxygen leakage through the flame zone is on the order of $X_{O2} \approx 0.012$.

After the radiative extinction of the high-temperature diffusion flame occurs at t = 7 s, the temperature decreases in the entire field, thus the oxygen penetrates into the near-burner region, and the low-temperature cool-flame regime begins. Figure 2b shows the calculated structure at t = 24 s, just before re-ignition occurs. The peak HRR (2.1 ± 0.1 W/cm^3), which is comparable to that of the high-temperature flame, occurs at a constant temperature of 700 K in close proximity (≈1 mm) to the fuel source. Despite the non-spherical fuel source, the variation in the peak HRR location in the axial and radial directions is relatively small (0.9–1.2 mm). Furthermore, it is reasonable to maintain the constant fuel velocity (1 cm/s) because the experimentally determined burning-rate constant during the cool flame regime is only slightly smaller than that for the high-temperature diffusion flame [3]. The oxygen mole fraction in the cool flame zone is $X_{O2} \approx 0.006$.

After a relatively long period (≈18 s) of the cool flame regime, a flash re-ignition starts at a point farther outside the cool flame, the ignition kernel grows, and the flame-edge starts to propagate around the fuel source. Figure 2c shows the propagating flame at t = 25 s. The HRR contours shows that as the high-temperature diffusion flame surrounds the upper portion of the fuel source, the cool-flame zone inside disappears because the oxygen penetration is blocked by the consumption in the diffusion flame zone. Immediately after the diffusion flame surrounds the fuel source completely, extinction occurs as the combustible mixture is consumed and the fuel-oxygen concentration field is not re-established to form a steady diffusion flame.

Figure 3 shows the temporal variations in the calculated maximum temperature, the temperature at the maximum HRR, the maximum HRR, the total HRR, and the radial flame location across the burner center (z = 0) in the zero-gravity n-heptane flame in quiescent air. The variations in the axial direction upstream and downstream along the burner center (r = 0) (not shown) are similar. The flame temperature and the HRR decrease from 1629 K to 1234 K and from 2.6 W/cm^3 to 1.8 W/cm^3, respectively, during t = 1 s to t = 6 s, as the flame weakens.

The diffusion flame extinction occurs at ≈1200 K, at which the main heat-release step CO + OH → CO_2 +H shuts off. During the low-temperature cool-flame regime, the temperature at the

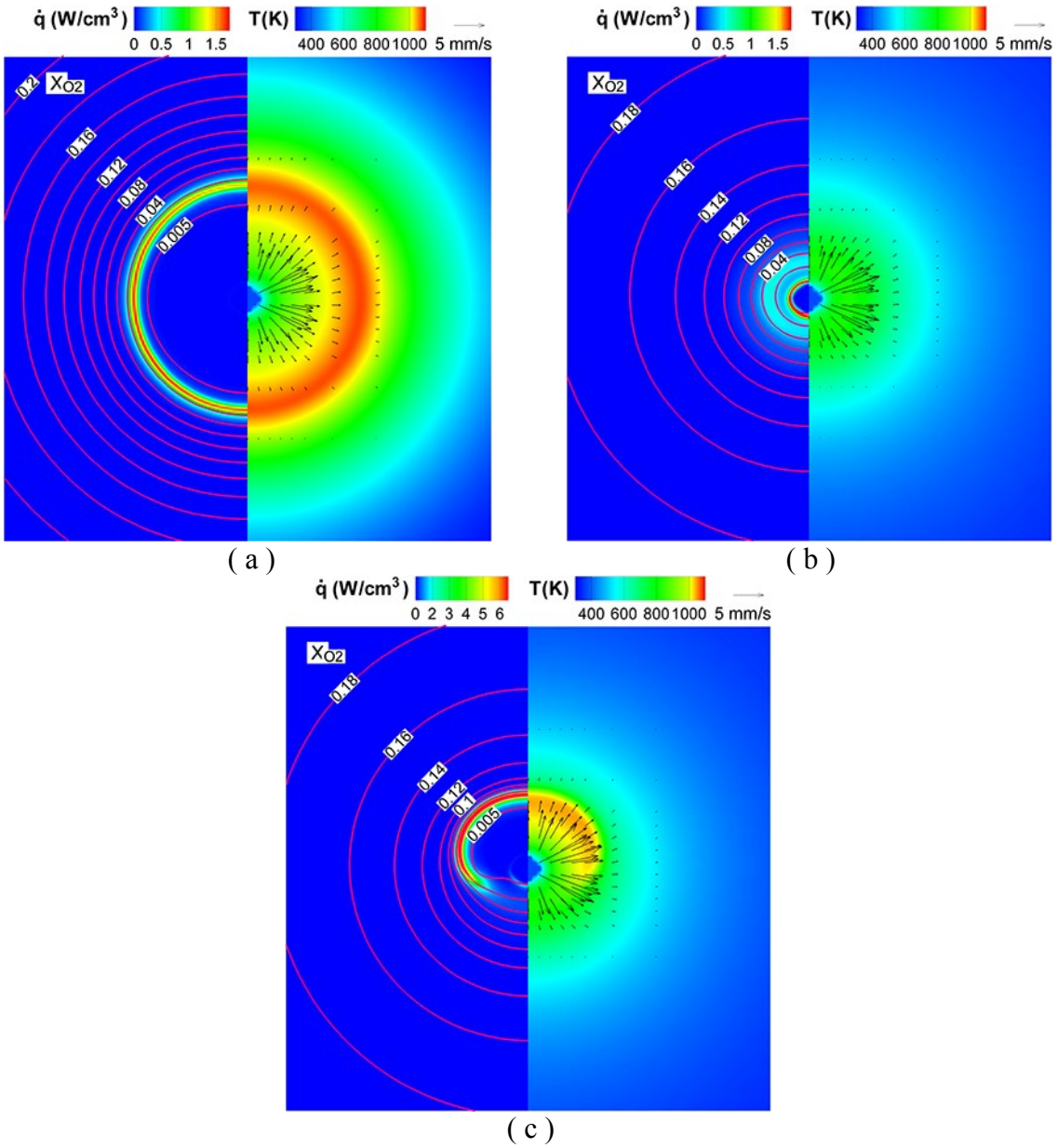

Figure 2: Calculated structure of zero-gravity n-heptane flames in quiescent air (the field of view: 80 mm × 80 mm): (a) near-extinction diffusion flame, t = 6 s; (b) near-reignition cool flame, t = 24 s; and (c) reignited propagating flame, t = 25 s

maximum HRR remains constant at ≈700 K, while the maximum temperature increases slightly around 800 K. The maximum HRR of the cool flame increases to the level comparable to the high-temperature diffusion flame and then decreases until the re-ignition occurs at t = 25 s, when all variables exhibit sharp peaks. Figure 3b shows a remarkable correlation of the total HRR integrated over the entire flame with the flame radius (and, in turn, the flame surface area).

Figure 4 shows the radial distributions of the calculated temperature and HRR across the burner center (z = 0) in the zero-gravity n-heptane flame in quiescent air at different times. The temperature and HRR peak values decrease and their radial locations increase as the flame

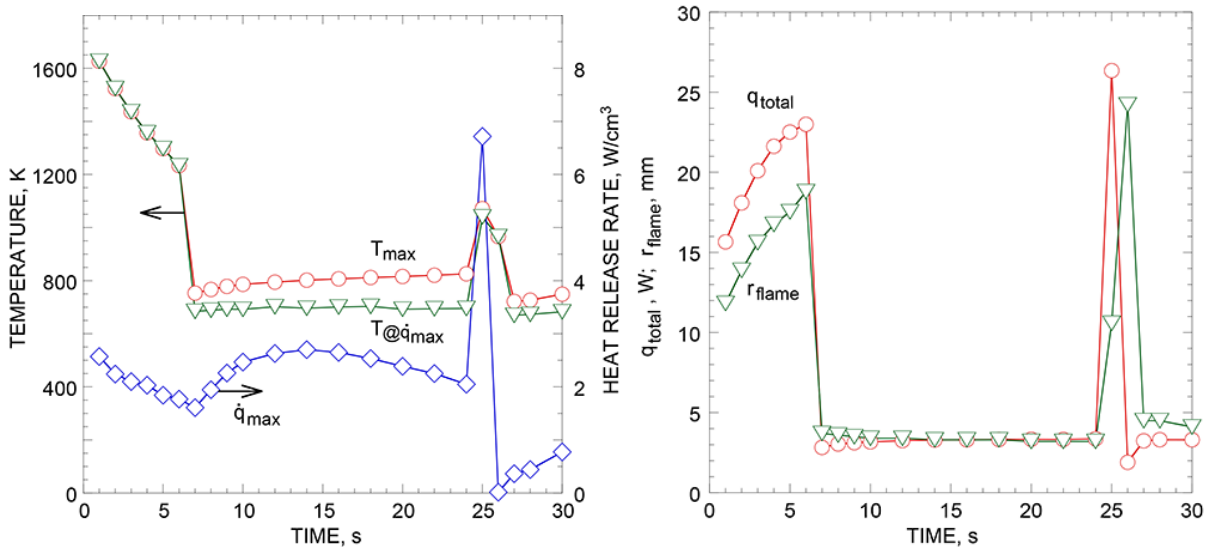

Figure 3: Temporal variations in (a) the calculated maximum temperature, the temperature at the maximum HRR, and the maximum HRR; and (b) the total HRR and the radial flame location across the burner center ($z = 0$) in the zero-gravity n-heptane flame in quiescent air

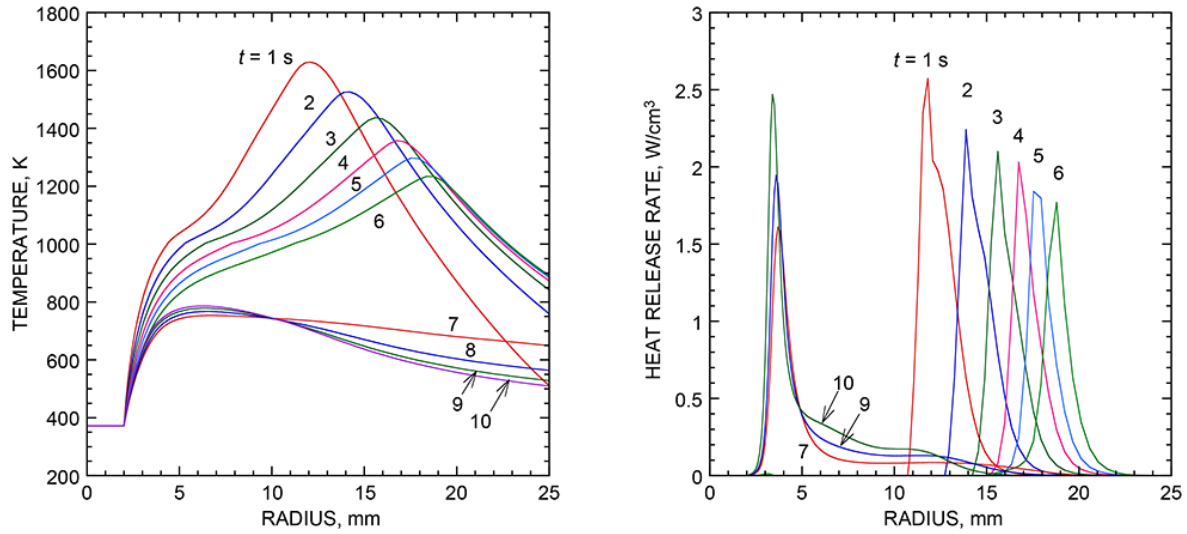

Figure 4: Radial distributions of (a) the calculated temperature and (b) the HRR across the burner center ($z = 0$) in the zero-gravity n-heptane flame in quiescent air

weakens and expands outwardly until $t = 6$ s. As the radiative extinction of the high-temperature diffusion flame occurs, the temperature decreases rapidly in the entire area and the HRR peak disappears. At $t = 7$ s, the HRR peak appears in close proximity of the burner surface. Thus, the transition from the high-temperature to low-temperature combustion regime occurs discretely, instead of a propagation of a flame front, because the oxygen must diffuse through the relatively low temperature zone to reach the burner surface. Furthermore, although the cool flame temperature (700 K) is much lower than that of the high-temperature diffusion flame (1200–1600 K), the temperature gradient at the burner surface ($r =$ 2 mm) in the cool flame at $t = 10$ s is nearly the same as that for the high-temperature flame at $t = 6$ s just before the extinction. This

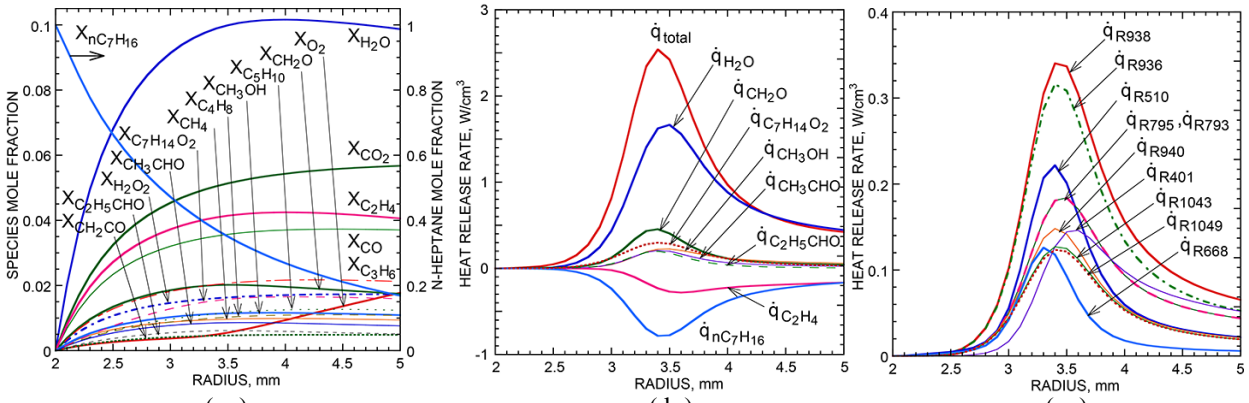

(a) (b) (c)

Figure 5: (a) Calculated species mole fractions, (b) the HRR per species formation, and (c) the HRR per reaction step across the burner center (z = 0) at t = 10 s in the low-temperature cool-flame regime in the zero-gravity n-heptane flame in quiescent air

result implies that the heat feedback from the flame to the burner surface is maintained at a comparable level before and after the transition to the cool-flame burning regime. It is consistent with the experimental result that the burning-rate constant during the cool-flame regime is only slightly lower than that for the high-temperature diffusion flame regime.

Figure 5 shows the calculated species mole fractions, the HRR per species formation, and the HRR per reaction step in the low-temperature cool-flame regime at t = 10 s. The peak HRR is located at r = 3.4 mm, which is 1.4 mm from the burner surface. Figure 5a shows that n-heptane diffuses from the fuel source outwardly and the oxygen diffuses from the ambient inwardly as driven by their concentration gradients. The mole fractions of n-heptane and oxygen at the reaction zone (at the peak HRR) are $X_{\text{n-C7H16}}$ = 0.37 and X_{O2} = 0.0048, respectively. Thus, a substantial amount of the unburned fuel escapes through the cool flame zone. The H_2O mole fraction peaks (X_{H2O} = 0.1) near the reaction zone. Figure 5b reveals that the formation of H_2O is the major contributor to the heat release rate. Other important species include aldehydes, methanol, and $C_7H_{14}O_2$. Figure 5c identifies further the main reaction steps that contribute to the heat-release rate. The main heat-release contributing reaction steps are as follows.

$$C_7H_{15} + O_2 \rightarrow C_7H_{15}O_2 \qquad \text{(R938, R936, R940)}$$

$$nC_3H_7 + O_2 \rightarrow C_3H_7O_2 \qquad \text{(R510)}$$

$$nC_7H_{16} + OH \rightarrow C_7H_{15} + H_2O \qquad \text{(R795, R793, R797)}$$

$$C_2H_5 + HO_2 \rightarrow C_2H_5O + OH \qquad \text{(R401)}$$

$$C_7H_{14}OOH \rightarrow C_7H_{14}O + OH \qquad \text{(R1043)}$$

$$C_7H_{14}OOH \rightarrow C_7H_{14}O + OH \qquad \text{(R1049)}$$

$$pC_4H_9 + O_2 \rightarrow C_4H_9O_2 \qquad \text{(R668)}$$

$$HCO + O_2 \rightarrow CO + HO_2 \qquad \text{(R91)}$$

$$CH_3 + O_2 + M \rightarrow CH_3O_2 + M \qquad \text{(R380)}$$

$$C_2H_5 + O_2 \rightarrow C_2H_5O_2 \qquad \text{(R378)}$$

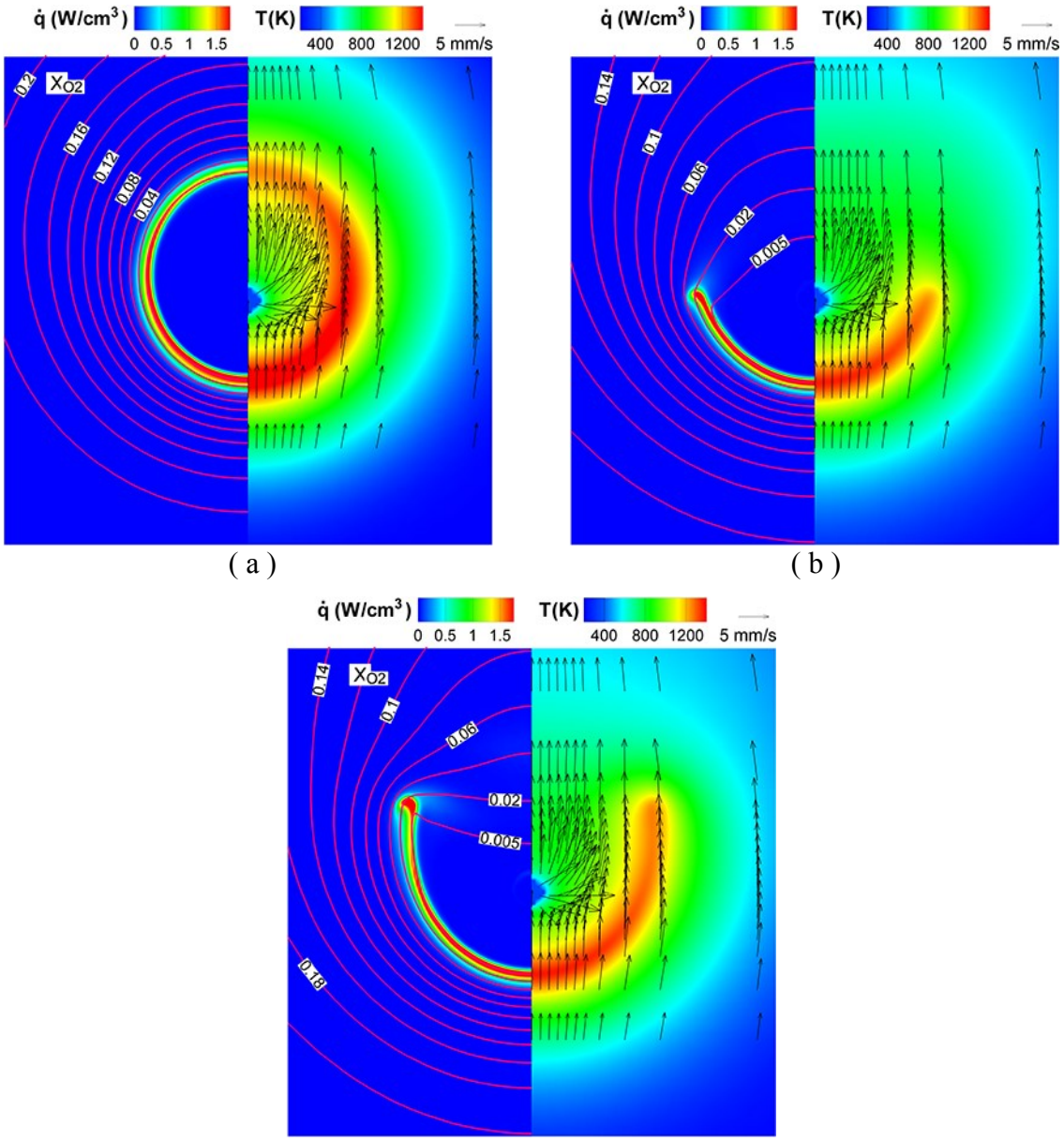

Figure 6: Calculated structure of zero-gravity n-heptane flames in airstream (3 mm/s): (a) stable flame, t = 4 s; (b) pulsating flame (receded), t = 19 s; and (c) pulsating flame (propagating), t = 20 s

Flame-Flow Interactions

Figure 6 shows the calculated structure of zero-gravity n-heptane flames in airstream at 3 mm/s. Figure 6a is a stable flame at t = 4 s. The flame is slightly elongated downstream by the flow. The combustion is enhanced in the upstream region, as a result of the convective influx of the oxygen in addition to diffusion. On the other hand, in the downstream region, the convective fuel flux and the oxygen diffusion against the flow reduce the combustion. Thus, the temperature and HRR increase in the upstream region and reduce in the downstream region. As a result, a local extinction occurs downstream. The flame edge recedes forward (upstream) and then propagates backward, thus leading to regular flame oscillations. Figure 6b shows the

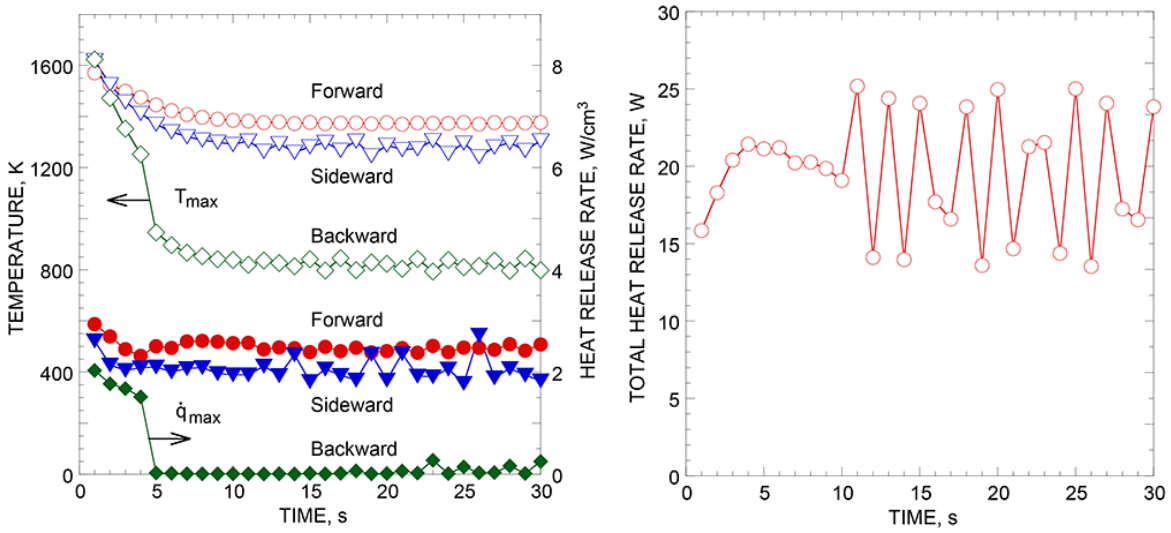

Figure 7: Temporal variations in (a) the calculated maximum temperature and the maximum

receded flame at t = 19 s. Because of the combustion enhancement by the airstream in the upstream region, the flame zone is stabilized at relatively high temperature. As the fuel-air mixing progresses downstream, the flame edge propagates backward. Figure 6c shows the propagating flame. The edge of the propagating flame is particularly enhanced. Although the flame is open toward downstream, no cool flame is formed, probably due to the flow of combustion products against the oxygen diffusion. The X_{O2} = 0.005 contour curve cannot reach the near surface location to form the cool flame.

Figure 7 shows the temporal variations in the calculated maximum temperature, the maximum HRR in the forward (upstream), side ward, and backward (downstream) directions; and the total HRR in the zero-gravity n-heptane flame in airstream at 3 mm/s. Figure 7a shows that the maximum temperature and the maximum HRR decrease initially, particularly in the backward region, thus resulting in the local extinction downstream at t = 5 s. Figure 7b reveals that the total heat release varies up and down in response to flame pulsations at 0.42 Hz. At higher airstream velocities (4 to 10 mm/s) (not shown), pulsations do not occur and the locally extinguished flame become steady state.

4. Conclusions

The axisymmetric 2D simulations of gaseous n-heptane flames in a quiescent or convective-air zero-gravity environment have provided insights into a series of distinct combustion phenomena. The calculated combustion characteristics change dramatically with the air velocity as follows.

1. In a quiescent air environment, a spherical diffusion flame expands, radiative heat losses increase, the local HRR and flame temperature decrease, and the flame extinguishes eventually at ≈1200 K, at which the main heat-release step CO + OH → CO_2 +H shuts off.
2. The radiative extinction of the visible diffusion flame is followed by a transition to the low-temperature (≈700 K) "cool-flame" combustion regime, as a result of the negative temperature coefficient in the low-temperature chemistry, with the heat release (from H_2O formation reactions, etc.) in close proximity to the fuel source.

3. The calculated high concentrations of n-heptane (X_{nC7H16} = 0.37) and water vapor (X_{H2O} = 0.1) in the cool flame zone suggest that the vapor cloud experimentally observed after the total extinction of the cool flame is likely due to the condensation of the fuel-H_2O mixture.
4. The calculated temperature gradients at the burner surface (and, in turn, the heat feedback) are comparable for the visible diffusion flame and the cool flame; it is consistent with the experimental observation that the burning rate constant decreases only slightly.
5. The simulation shows that, after a relatively long period of the low-temperature cool-flame regime, flash re-ignition, flame-edge propagation, and extinction of the re-ignited flame occur.
6. In a low-speed (≈3 mm/s) airstream, the calculated diffusion flame is enhanced upstream and experiences a local extinction downstream at ≈1200 K, followed by steady flame pulsations (≈0.4 Hz).
7. At higher air velocities (4–10 mm/s), the calculated locally extinguished flame becomes steady state.
8. The computation does not show the low-temperature cool flame co-existing with the high-temperature diffusion flame (either the stable, locally extinguished, or pulsating flames) because the oxygen cannot penetrate to the burner surface due to the consumption by the high-temperature flame or the convection against the oxygen diffusion.

5. Acknowledgements

This work was supported by the NASA Space Life and Physical Sciences Research and Applications Division (SLPSRA). The authors would like to thank Daniel Dietrich, Vedha Nayagam, and Forman Williams for the fruitful discussion. We acknowledge Tanvir Farouk and Frederick Dryer for providing the reduced Curran n-heptane reaction mechanism.

6. References

[1] F.A. Williams, Combustion Theory, Benjamin/Cummings Publishing, Menlo Park California, 1985, p. 52.
[2] M.Y. Choi, F.L. Dryer, in: H.D. Ross (Ed.), Microgravity Combustion: Fire in Free Fall, Academic Press, San Diego, California, 2001, pp. 183-297.
[3] V. Nayagam, D.L. Dietrich, P.V. Ferkul, M.C. Hicks, F.A. Williams, Combust. Flame 159 (2012) 3583-3588.
[4] A. Cuoci, A. Frassoldati, T. Faravelli, E. Ranzi. Cool flames in droplet combustion, XXXVI Meeting of the Italian Section of the Combustion Institute, 2013.
[5] T.I. Farouk, F.L. Dryer, Combust. Flame 161 (2014) 565-581.
[6] T.I. Farouk, F.L. Dryer, Proc. Combust. Inst. 35 (2016), in press.
[7] V.R. Katta, L.P. Goss, W.M., Roquemore, AIAA Journal 32 (1994). 84.
[8] W.M. Roquemore, V.R. Katta, J. Visualization 2 (2000) 257-272.
[9] H. J. Curran, P. Gaffuri, W. J. Pitz, C. K. Westbrook, Combust. Flame 114 (1998) 149 -177.
[10] V.R. Katta, S.K. Aggarwal, W.M. Roquemore, Fuel, 93 (2012) 339-350.
[11] P.Berta, S.K. Aggarwal, I.K. Puri, Combust. Flame 145, (2006) 740-764.
[12] Anon., Computational Submodels, International Workshop on Measurement and Computation of Turbulent Nonpremixed Flames, 2001. http://www.ca.sandia.gov/TNF/rdiation.html.
[13] R.P. Lindstedt, in: H. Bockhorn (Ed.), Soot Formation in Combustion: Mechanisms and Models, Springer-Verlag, Heidelberg, 1994, pp.417-439.
[14] K.M. Leung, R.P. Lindstedt, W.P. Jones, Combust. Flame 87 (1991) 289-305.